Draft version July 20, 2015
Preprint typeset using LaTeX style emulateapj v. 11/10/09

C/O AND SNOWLINE LOCATIONS IN PROTOPLANETARY DISKS: THE EFFECT OF RADIAL DRIFT AND VISCOUS ACCRETION

Ana-Maria A. Piso[1], et al.

Draft version July 20, 2015

ABSTRACT

The C/O ratio is an important signature of giant planet atmospheric composition and disk chemistry. We explore the effect of radial drift of solids and viscous gas accretion onto the central star on the snowline locations of the main C and O carriers in a protoplanetary disk, H_2O, CO_2 and CO, and the resulting C/O ratio in gas and dust throughout the disk. We determine the snowline locations for a range of fixed initial particle sizes, in both an active and a passive disk. We find that grains with sizes sizes $\sim$0.5 cm $\lesssim s \lesssim$ 7 m for a passive disk and $\sim$0.001 cm $\lesssim s \lesssim$ 7 m for an active disk desorb instantaneously and at a fixed size-dependent location in the disk regardless of the particle's initial position. The snowline location move inwards as the particle size increases, and the innermost snowlines are set by grains with initial size $s \sim 7$ m. Compared to a static disk, we find that radial drift and gas accretion move the H_2O and CO_2 snowlines inwards by up to 60 %, and the CO snowline by up to 50 %. We thus determine an inner limit on the snowline locations when radial drift and gas accretion are accounted for. Our results have direct implications on the C/O ratio in giant planet atmospheres that have formed in situ.

1. INTRODUCTION

The chemical composition of the atmospheres of giant planets can provide important constraints on their formation, accretion and migration history. These processes are tightly linked to the structure and evolution of the protoplanetary disk in which such planets form. It is thus essential to understand the disk chemistry and dynamics well enough to predict the types of planet compositions that result from planet formation in different parts of the disk, as well as backtrack the planet formation location based on planet compositions.

In recent years, the onset and development of sensitive infrared and (sub)millimeter spectroscopic observations has facilitated the detection of organic molecules in the outer regions of protoplanetary disks (e.g., Öberg et al. 2010, Öberg et al. 2011b, Öberg et al. 2011c). Of particular importance are volatile compounds, such as H_2O, CO_2, CO, N_2 etc. Recent detections of the snowlines of volatiles (such as the CO snowline, Qi et al. 2011) are significant, since the snowline locations of these molecules determine their relative abundance in gaseous and solid form in the protoplanetary disk, and thus the chemical composition of nascent giant planets.

An important signature of disk chemistry is the carbon-to-oxygen (C/O) ratio, as it provides information about the relative abundances of the main C and O carrier species. While the gas C/O ratio in disks may be potentially observable (Du et al. 2015), such detections do not yet exist. However, we can indirectly infer the relative abundance of disk C and O using detections of C/O ratios in exoplanet atmospheres. Spectroscopic observations of gas giants such as WASP-12b have found atmospheric C/O ratios close to unity, substantially different from the Solar value of 0.54 (Madhusudhan et al. 2011). One explanation for this discrepancy was proposed by Öberg et al. (2011a), who considered the fact that the main carries of carbon and oxygen, i.e. H_2O, CO_2 and CO, have different condensation temperatures. This changes the relative abundance of C and O in gaseous and solid form as a function of the snowline location of the volatiles mentioned above. Öberg et al. (2011a) calculated analytically the C/O ratio in gas in dust as a function of semimajor axis for passive protoplanetary disks and reproduced a gas C/O ratio of order unity between the CO_2 and CO snowlines, where oxygen gas is highly depleted.

Öberg et al. (2011a) assume a static disk with passive chemistry. In reality, additional dynamical and chemical processes affect the snowline locations and the resulting C/O ratio. Several works have addressed some of these effects. Madhusudhan et al. (2014) use a steady-state active disk model that includes planetary migration and use the C/O ratio to constrain migration mechanisms. Ali-Dib et al. 2014 calculate the C/O ratio throughout the disk by incorporating the evolution of solids, i.e. radial drift, sublimation and grain coagulation, as well as the diffusion of volatile vapors. Thiabaud et al. (2015) consider additional volatile species in their chemical network, such as N_2 or NH_3, and find that the C/O ratio may be enriched by up to four times the Solar value in certain parts of the disk.

Most studies of the C/O ratio in disks are particularly focused on the inner disk, in order to explain observations of super-stellar C/O ratios in the atmospheres of close-in exoplanets (Madhusudhan et al. 2011). In addition, the simultaneous inclusion of various dynamical and/or chemical processes makes it difficult to quantify the separate effect of each of these processes on snowline locations and the C/O ratio. In this paper, we focus on two particular dynamical effects, i.e. the radial drift of solids and viscous gas accretion. We enhance the model of Öberg et al. (2011a) by considering these two additional processes. We perform a systematic study to un-

[1] Harvard-Smithsonian Center for Astrophysics, 60 Garden Street, Cambridge, MA 02138

derstand the detailed qualitative and quantitative effects of radial drift and gas accretion on the H_2O, CO_2 and CO snowline locations, and the resulting C/O ratio in gas and dust throughout the protoplanetary disk. More importantly, we obtain a limit on how close to the star the snowline locations can be pushed by radial drift and gas accretion.

This paper is organized as follows. In Section 2, we present our disk, radial drift and desorption models, as well as the timescales relevant to the coupled drift-desorption process. We calculate the H_2O, CO_2 and CO snowline locations as a function of particle size for a passive and an active disk in Section 3, and the resulting C/O ratio throughout the disk in Section 4. In Section 5, we discuss the generality of our results, as well as additional effects on the snowline locations. Finally, we summarize our findings in Section 6.

2. MODEL FRAMEWORK

We present our protoplanetary disk model for both a passive and an active disk in section 2.1. In section 2.2, we describe our analytic model for the radial drift of solids. We summarize our ice desorption model in section 2.3. Finally, we discuss the relevant timescales for dynamical effects in the desorption process in section 2.4.

2.1. *Disk Model*

Passive disk. A passive disk is only irradiated by the central star and does not experience radial movement of gas or accretion heating. We adopt a minimum mass solar nebula (MMSN) disk model for a passive disk similar to the prescription of Chiang & Youdin (2010). The gas surface density and midplane temperature are

$$\Sigma_{\rm d} = 2000\,(r/{\rm AU})^{-1}\ {\rm g\ cm^{-2}} \tag{1a}$$

$$T_{\rm d} = 120\,(r/{\rm AU})^{-3/7}\ {\rm K}, \tag{1b}$$

where r is the semimajor axis. Based on some observations of protoplanetary disks (Andrews et al. 2010), our surface density profile, $\Sigma_{\rm d} \propto r^{-1}$, is flatter than that of Chiang & Youdin (2010), i.e. $\Sigma_{\rm d} \propto r^{-3/2}$.

Active disk with passive temperature profile. The gas is accreting onto the central star in an active disk, which causes the gas surface density to decrease with time. We model the active disk as a thin disk with an α-viscosity prescription (Shakura & Sunyaev 1973):

$$\nu = \alpha c_{\rm d} H_{\rm d}. \tag{2}$$

Here ν is the kinematic viscosity, $\alpha < 1$ is a dimensionless coefficient and we choose $\alpha = 0.01$, and $c_{\rm d}$, $H_{\rm d}$ are the isothermal sound speed and disk scale height, respectively:

$$c_{\rm d} = \sqrt{\frac{k_{\rm B}T_{\rm d}}{\mu m_{\rm p}}} \tag{3a}$$

$$H_{\rm d} = \frac{c_{\rm d}}{\Omega_{\rm k}}, \tag{3b}$$

where $k_{\rm B}$ is the Boltzmann constant, μ is the mean molecular weight of the gas, $m_{\rm p}$ is the proton mass, and $\Omega_{\rm k} \equiv \sqrt{GM_*/r^3}$ is the Keplerian angular velocity, with G the gravitational constant and M_* the stellar mass. We choose $M_* = M_\odot$ and $\mu = 2.35$, corresponding to the Solar composition of hydrogen and helium. The temperature profile for an active disk is assumed to be the same as for the passive disk and given by Equation (1b). From Equations (2) and (3), the viscosity can thus be expressed as a power-law in radius, $\nu \propto r^\gamma$, with $\gamma = 15/14 \approx 1$ for our choice of parameters. Following Hartmann et al. (1998), we define $R \equiv r/r_{\rm c}$ and $\nu_{\rm c} \equiv \nu(r_{\rm c})$, where $r_{\rm c}$ is a characteristic disk radius. We choose $r_{\rm c} = 100$ AU. The gas surface density is then given by the self-similar solution

$$\Sigma_{\rm d}(R,T) = \frac{M_{\rm d}}{2\pi r_{\rm c}^2 R^\gamma} T^{(-5/2-\gamma)/(2-\gamma)} \exp\Big[-\frac{R^{-(2-\gamma)}}{T}\Big], \tag{4}$$

where $M_{\rm d}$ is the total disk mass and

$$T \equiv \frac{t}{t_{\rm c}} + 1 \tag{5a}$$

$$t_{\rm c} \equiv \frac{1}{3(2-\gamma)}\frac{r_{\rm c}^2}{\nu_{\rm c}}, \tag{5b}$$

where t is time. We choose $M_{\rm d} = 0.1 M_\odot$ (e.g., Birnstiel et al. 2012), but we note that our results are insensitive to this choice (see Section 5).

Active disk steady-state. A steady-state solution to the evolution of an actively accreting disk gives a gas surface density $\Sigma_{\rm d}$ and mass flux $\dot{M}$ that are constant in time and independent of semimajor axis. Since calculating the midplane temperature self-consistently for an active disk is non-trivial, we use instead the Shakura-Sunyaev thin disk steady-state solution to derive the midplane temperature profile, $T_{\rm d,act}$. The equations governing the evolution of the steady-state disk are listed in Appendix A. We assume an interstellar opacity for the dust grains given by Bell & Lin (1994), but reduced by a factor of 100. This reduction is due to the fact that disk opacities are lower than the interstellar one. The scaling is consistent with more detailed models of grain opacities in disks (e.g., Mordasini et al. 2014). Our opacity law is thus

$$\kappa = \kappa_0 T_{\rm d,act}^2, \tag{6}$$

where $\kappa_0 = 2 \times 10^{-6}$. By solving the Equation set (A1) we find

$$T_{\rm d,act} = \frac{1}{4r}\Big(\frac{3G\kappa_0 \dot{M}^2 M_* \mu m_{\rm p} \Omega_{\rm k}}{\pi^2 \alpha k_{\rm B} \sigma}\Big)^{1/3}. \tag{7}$$

However, both accretion heating and stellar irradiation contribute to the thermal evolution of the disk. We thus compute the midplane temperature for our steady-state active disk as

$$T_{\rm d}^4 = T_{\rm d,act}^4 + T_{\rm d,pas}^4, \tag{8}$$

where to avoid notation confusion $T_{\rm d,pas} = T_{\rm d}$ from Equation (1b), the temperature profile for an active disk. We can then easily determine $c_{\rm d}$ and $H_{\rm d}$ from Equation (3), as well as the viscosity ν from Equation (2) for a given α. For consistency, we choose $\alpha = 0.01$ as in the previous case. Finally, we determine $\Sigma_{\rm d}$ from Equation (A1g), where we choose $\dot{M} = 10^{-8} M_\odot\ {\rm yr}^{-1}$ based on disk observations (e.g., Andrews et al. 2010). We note that $\Sigma_{\rm d}$ is no longer constant when stellar irradiation is

taken into account in the active disk steady-state solution.

Static disk. To compare our results with those of Öberg et al. (2011a), we also use a static disk model, with $\Sigma_{\rm d}$ and $T_{\rm d}$ described by Equations (1a) and (1b). The static model does not take into account gas accretion on to the central star or radial drift of solids (see Section 2.2).

2.2. *Radial Drift*

Solid particles in orbit their host star at the Keplerian velocity $v_{\rm k} \equiv \Omega_{\rm k} r$. The gas, however, experiences an additional pressure gradient, which causes it to rotate at sub-Keplerian velocity (Weidenschilling 1977). Dust grains that are large enough thus experience a headwind, which removes angular momentum, causing the solids to spiral inwards and fall onto the host star. Small particles are well-coupled to the gas, while large planetesimals are decoupled from the gas. From Chiang & Youdin (2010), the extent of coupling is quantified by the dimensionless stopping time, $\tau_{\rm s} \equiv \Omega_{\rm k} t_{\rm s}$, where $t_{\rm s}$ is

$$t_{\rm s} = \begin{cases} \rho_{\rm s} s/(\rho_{\rm d} c_{\rm d}), & s < 9\lambda/4 \quad \text{Epstein drag} \\ 4\rho_{\rm s} s^2/(9\rho_{\rm d} c_{\rm d} \lambda), & s < 9\lambda/4,\ {\rm Re} \lesssim 1 \quad \text{Stokes drag.} \end{cases} \tag{9}$$

Here $\rho_{\rm d}$ is the gas midplane density, $\rho_{\rm s} = 2$ g cm^{-3} is the density of a solid particle, s is the particle size, λ is the mean free path, and Re is the Reynolds number.

For a passive disk, the radial drift velocity can be approximated analytically as

$$\dot{r} \approx -2\eta\Omega_{\rm k} r \Big(\frac{\tau_{\rm s}}{1+\tau_{\rm s}^2}\Big), \tag{10}$$

where

$$\eta \equiv -\frac{\partial P_{\rm d}/\partial \ln r}{2\rho_{\rm d} v_{\rm k}^2} \approx \frac{c_{\rm d}^2}{2v_k^2} \tag{11}$$

and $P_{\rm d} = \rho_{\rm d} c_{\rm d}^2$ is the disk midplane pressure.

For an active disk, the radial drift velocity has an additional term due to the radial movement of the gas, i.e.

$$\dot{r} \approx -2\eta\Omega_{\rm k} r \Big(\frac{\tau_{\rm s}}{1+\tau_{\rm s}^2}\Big) + \frac{\dot{r}_{\rm gas}}{1+\tau_{\rm s}^2}, \tag{12}$$

where $\dot{r}_{\rm gas}$ is the radial gas accretion velocity and can be expressed as (e.g., Frank et al. 2002)

$$\dot{r}_{\rm gas} = -\frac{3}{\Sigma_{\rm d}\sqrt{r}} \frac{\partial}{\partial r}(\nu\Sigma_{\rm d}\sqrt{r}) \tag{13}$$

with $\Sigma_{\rm d}$ from Equation (4). For the active disk steady-state solution (see Section 2.1), $\dot{r}_{\rm gas}$ can be expressed more simply using the definition of the mass flux, $\dot{M} = -2\pi r \dot{r}_{\rm gas} \Sigma_{\rm d}$, with $\dot{M}$ fixed and $\Sigma_{\rm d}$ obtained from Equation (A1g).

2.3. *Volatile Desorption*

In order for a volatile species to thermally desorb, it has to overcome the binding energy that keeps it on the grain surface. Following Hollenbach et al. (2009), the desorption rate per molecule for a species x can be expressed as

$$R_{\rm des,x} = \nu_x \exp\left(-E_x/T_{\rm grain}\right), \tag{14}$$

where E_x is the adsorption binding energy in units of Kelvin, $T_{\rm grain}$ is the grain temperature, and $\nu_x = 1.6\times10^{11}\sqrt{(E_x/\mu_x)}$ s^{-1} is the molecule's vibrational frequency, with μ_x the mean molecular weight. We assume that the dust and gas have the same temperature in the disk midplane, hence $T_{\rm grain} = T_{\rm d}$. For H_2O, CO_2 and CO, the binding energies E_x are assumed to be 5800 K, 2000 K and 850 K, respectively (Öberg et al. 2011a). We use the desorption rate, $R_{\rm des}$, to estimate the desorption timescale for particles of different sizes as described in section 2.4.

2.4. *Relevant Timescales*

We can estimate the extent to which radial drift and gas accretion affect desorption by comparing the timescales for desorption, drift and accretion, for solids of different sizes and compositions.

Desorption timescale. We assume that the solid bodies are perfect spheres and are entirely composed of only one volatile species, i.e. either H_2O, CO_2 or CO [2]. The desorption timescale can then be estimated as

$$t_{\rm des} = \frac{\rho_{\rm s}}{3\mu_x m_{\rm p}} \frac{s}{N_x R_{\rm des,x}}, \tag{15}$$

where $N_x \approx 10^{15}$ sites cm^{-2} is the number of adsorption sites of volatile x per cm^2 (Hollenbach et al. 2009).

Radial drift timescale. To order of magnitude, the radial drift timescale can be estimated as

$$t_{\rm r,drift} \sim \Big|\frac{r}{\dot{r}}\Big|, \tag{16}$$

where $\dot{r}$ is the radial drift velocity given by Equation (10) for a passive disk and by Equation (12) for an active disk.

Gas accretion timescale. The timescale for gas accretion onto the central star for an active disk is (e.g., Armitage 2010)

$$t_{\rm gas,acc} \sim \frac{r^2}{\nu} \sim \frac{1}{2\alpha\eta\Omega_{\rm k}}, \tag{17}$$

with the latter expression derived from Equations (2) and (11).

For simplicity purposes, we calculate the radial drift timescale, $t_{\rm r,drift}$, for a passive disk in this section, but most of our conclusions hold true for an active disk as well. Figure 1 shows $t_{\rm des}$, $t_{\rm r,drift}$ and $t_{\rm gas,acc}$ as a function of particle size at three different locations in the disk, corresponding to the H_2O, CO_2 and CO snowlines in the static disk. As expected, micron-sized particles desorb on very short timescales of $\sim 1-1000$ years in the close vicinity of their respective snowlines, since the desorption rate depends exponentially on temperature and hence on disk location (see Equation 14). On the other hand, their radial drift timescale exceeds the typical disk lifetime of a few Myr by several orders of magnitude due to their strong coupling with the gas. Thus for small particles in a passive disk, the snowline locations and the C/O ratio are the same as for a static disk (see Figure 1 from Öberg et al. 2011a) [3]. At the other extreme, kilometer-sized particles are unaffected by gas drag and have long

[2] We discuss the validity of these simplifications in section 5.

[3] This is not true for an active disk, however, where gas accretion causes even micron-sized particles to drift significantly before desorbing, as we show in section 3.

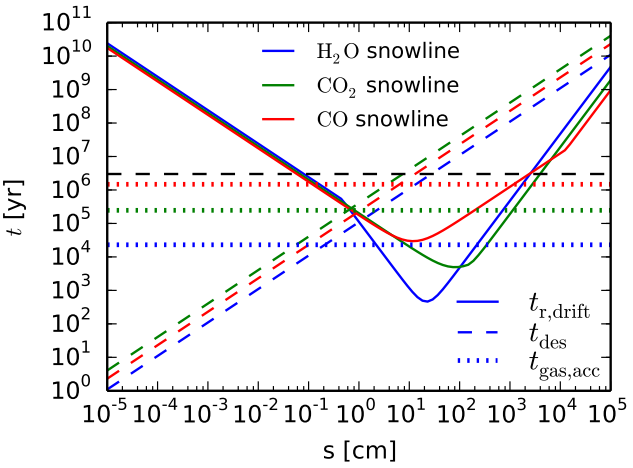

FIG. 1.— Relevant timescales for dynamical effects in the desorption process: $t_{\rm r,drift}$ (solid lines), $t_{\rm des}$ (dashed lines) and $t_{\rm gas,acc}$ (dotted lines). The timescales are calculated at three representative locations, i.e. the H_2O, CO_2 and CO snowlines in the static disk. For our choice of parameters, the snowlines are located at ∼0.7 AU (blue lines), ∼8.6 AU (green lines) and ∼59 AU (red lines), respectively. The horizontal dashed line represents a typical disk lifetime of 3 Myr. Radial drift and gas accretion affect desorption in the regions where their respective timescales, i.e. $t_{\rm r,drift}$ and $t_{\rm gas,acc}$, are comparable to the desorption timescale $t_{\rm des}$.

desorption timescales (≫1 Myr), and the snowline locations and C/O ratio remain unchanged in this case as well. This is true for both passive and active disks, since large planetesimals are decoupled from the gas and hence unaffected by gas accretion onto the host star.

Of particular interest for our purposes is the particle size regime for which (1) $t_{\rm r,drift} \lesssim t_{\rm des} \lesssim t_{\rm d}$ ($t_{\rm d}$ = 3 Myr is the disk lifetime), i.e. for ∼0.5 cm $\lesssim s \lesssim$ 1000 cm, or (2) $t_{\rm gas,acc} \lesssim t_{\rm des} \lesssim t_{\rm d}$, i.e. for ∼0.1 cm $\lesssim s \lesssim$ 10 cm. In these cases, radial drift or gas accretion (or both) are faster than thermal desorption. We note that $t_{\rm gas,acc} < t_{\rm d}$ always holds true. Particles of sizes that satisfy the requirements above will drift significantly due to radial drift or gas accretion before desorbing, thus moving the H_2O, CO_2 and CO snowlines closer towards the central star and changing the C/O ratio throughout the disk. We quantify these effects in sections 3 and 4.

3. SNOWLINE LOCATIONS

In this section we use the model described in section 2 to quantify the effects of radial drift (passive disk) or radial drift and gas accretion (active disk) on the snowline location, for dust particles of different sizes composed of either H_2O, CO_2 or CO. Specifically, we determine a particle's final location (i.e., where the particle either fully desorbs or remains at its initial size due to a long desorption timescale) as a function of its initial position in the disk, after the gas disk has dissipated. The disk lifetime, $t_{\rm d}$, is particularly relevant since this is the timescale on which giant planets form. The snowline locations at $t = t_{\rm d}$ throughout the protoplanetary disk determine the disk C/O ratio in gas at this time, and thus the C/O ratio in giant planet atmospheres that have formed *in situ*.

For each species x, we determine the final location in the disk of a particle of initial size s_0 by solving the following system of coupled differential equations:

$$\frac{ds}{dt} = -\frac{3\mu_x m_{\rm p}}{\rho_{\rm s}} N_x R_{\rm des,x} \quad (18a)$$

$$\frac{dr}{dt} = \dot{r}, \quad (18b)$$

where the desorption rate $R_{\rm des,x}$ for each particle type (i.e., composed of H_2O, CO_2 or CO) is evaluated at $T = T_{\rm d}(r)$, and the radial drift velocity $\dot{r}$ is given by Equation (10) for a passive disk and Equation (12) for an active disk. Equations (18a) and (18b) describe the coupled desorption and radial drift, and can be derived straightforwardly from Equation (15). Our boundary conditions are $s(t_0) = s_0$, $r(t_0) = r_0$, and $s(t_{\rm d}) = 0$, where t_0 is the initial time at which we start the integration and r_0 is the initial location of the particle. We choose t_0 = 1 year, but our result is independent on the initial integration time as long as $t_0 \ll t_{\rm d}$.

We define the final position of a grain as the disk location it has reached after $t_{\rm d}$ = 3 Myr, or the radius at which it completely desorbs if that happens after a time shorter than 3 Myr. Figure 2 shows our results for H_2O, CO_2 and CO particles, for both a passive and an active disk. We do not show the equivalent result for the steady-state active disk since the trends are qualitatively the same as for the active disk with the temperature profile given by Equation (1b), but we discuss the C/O ratio steady-state active disk results in Section 4. Kilometer-sized bodies do not drift or desorb during the disk lifetime neither for a passive nor for an active disk. Similarly, micron- to mm-sized particles in the passive disk do not drift or desorb unless they are located inside the static snowlines. This is not in contradiction with the desorption timescales for small particles from Figure 1, since small grains only desorb fast at or nearby their respective snowlines, as mentioned in Section 2.4. In an active disk, however, micron-to mm-sized grains do drift significantly since they move at the same velocity as the accreting gas. For 0.5 cm $\lesssim s_0 \lesssim$ 700 cm in a passive disk and 0.001 cm $\lesssim s_0 \lesssim$ 700 cm in an active disk, we notice that particles of initial size s_0 desorb at a fixed distance $r_{\rm des}$ regardless of their original location in the disk. In fact, the only grains that will both drift and evaporate are those that reach their fixed final location (represented by the horizontal curves in Figure 2) within the disk lifetime. We show in section 4 that this result is essential in determining the C/O ratio throughout the disk for different particle sizes.

Intuitively, this fixed $r_{\rm des}$ should be the location in the disk for which $t_{\rm r,drift} \sim t_{\rm des}$, given an initial particle size. We can calculate this location analytically by equating Equations (15) and (16) and solving for $r = r_{\rm des}(s)$ for a given particle size s. Figure 3 shows $r_{\rm des}$ calculated analytically using the prescription above as a function of the actual desorption distance calculated numerically, for the range of particle sizes that desorb at a fixed distance in a passive and an active disk (see Figure 2). We notice that the analytic approximation accurately reproduces the numerical result for most cases of interest, but it slightly deviates for particles larger than $s \gtrsim 10$ cm. For small particles with $\tau_{\rm s} \ll 1$, $t_{\rm r,drift}$ is a power-law in r (for our parameters, $t_{\rm r,drift} \propto r^{-1/14}$ for the passive disk), and

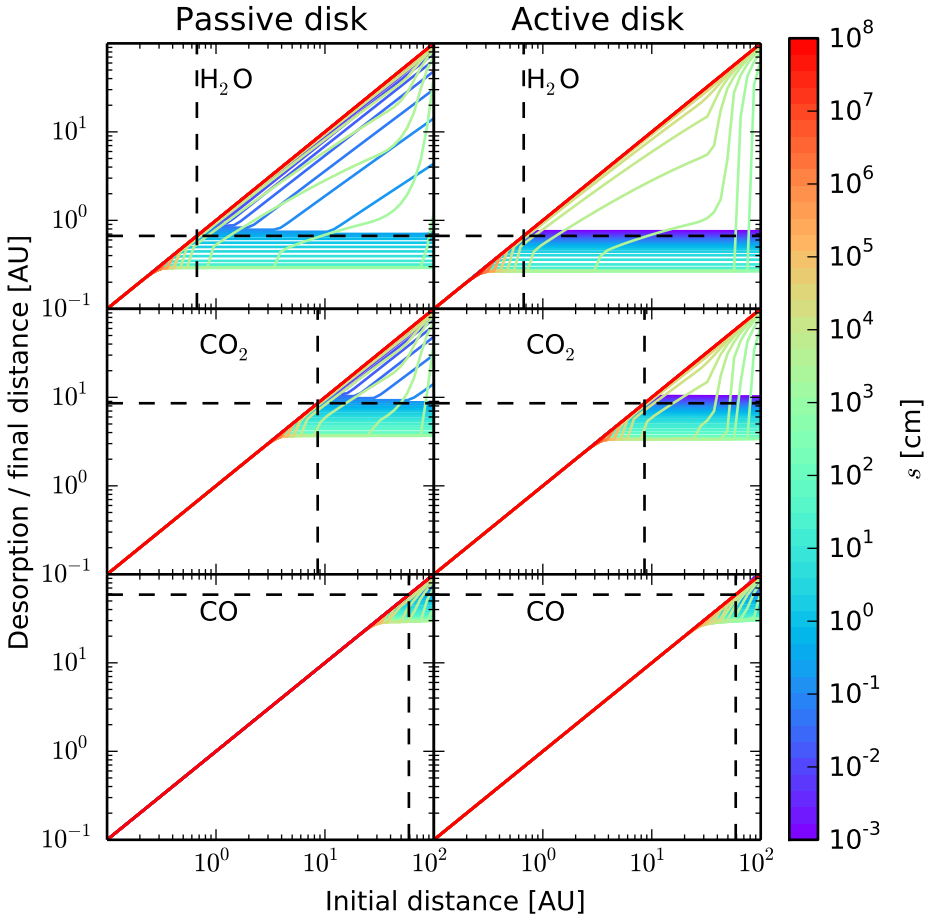

FIG. 2.— Desorption distance (if a grain fully desorbs) or final distance (if a grain does not fully desorb), as a function of a particle's initial location in the disk, for a range of particle sizes, and for both a passive disk (left panels) and an active disk (right panels). The desorption distance is calculated for particles composed of H_2O (top panels), CO_2 (middle panels) and CO (bottom panels). The particle size increases from 10^{-3} cm to 10^8 cm as indicated by the color bar. For a particle of a given initial size that entirely desorbs during $t_d = 3$ Myr, the desorption distance is the same regardless of the particle's initial location.

the Equation set (18) has an explicit analytic solution (see Appendix B). Once particles are large enough so that $\tau_s \sim 1$, $t_{r,drift}$ has a more complicated dependence on r (see Equation 9), and the coupled drift-desorption differential equations have to be integrated numerically to obtain an accurate result.

4. RESULTS FOR THE C/O RATIO

We now use our model and the results of Section 3 to determine the H_2O, CO_2 and CO snowline locations and the C/O ratio in disks with static chemistry that experience radial drift of solids and gas accretion on to the central star. Figure 4, left panels, shows the size evolution with time for H_2O particles of various initial sizes, starting at three different initial locations in a passive disk [4]. Solid H_2O particles evaporate almost instantly, although the time t_{des} at which a particle of a given initial size desorbs depends on its initial distance. A particle located at the initial time t_0 at a distance such that $t_{des} > t_d$ will therefore not desorb during the disk lifetime, but our model assumes that particles drift continuously at any location in the disk. The right panels of Figure 4 show that the drifting grains lose most of their mass in a very narrow distance range; moreover, this distance is the same for a given initial particle size, no matter where the particle started drifting at the time t_0 when the simulation is started. Figure 4 thus demonstrates that solid particles that drift and fully desorb during the lifetime of the protoplanetary disk do so (1) instantaneously, and (2) at a fixed stellocentric distance, regardless of their initial location in the disk. It follows that the H_2O, CO_2 and CO snowlines are fixed for a given initial particle size and disk model (passive or active). The C/O ratio will then only depend on disk properties, grain size, and the abundance of H_2O, CO_2 and CO relative to the H_2 abundance in the disk midplane.

We use the relative number densities of C and O in their different molecular forms (H_2O, CO_2 and CO) from Table 1 of Öberg et al. (2011a). Figure 5 shows the C/O ratio in gas and dust as a function of semimajor axis

[4] Our conclusions remain valid for an active disk and for particles composed of CO_2 or CO.

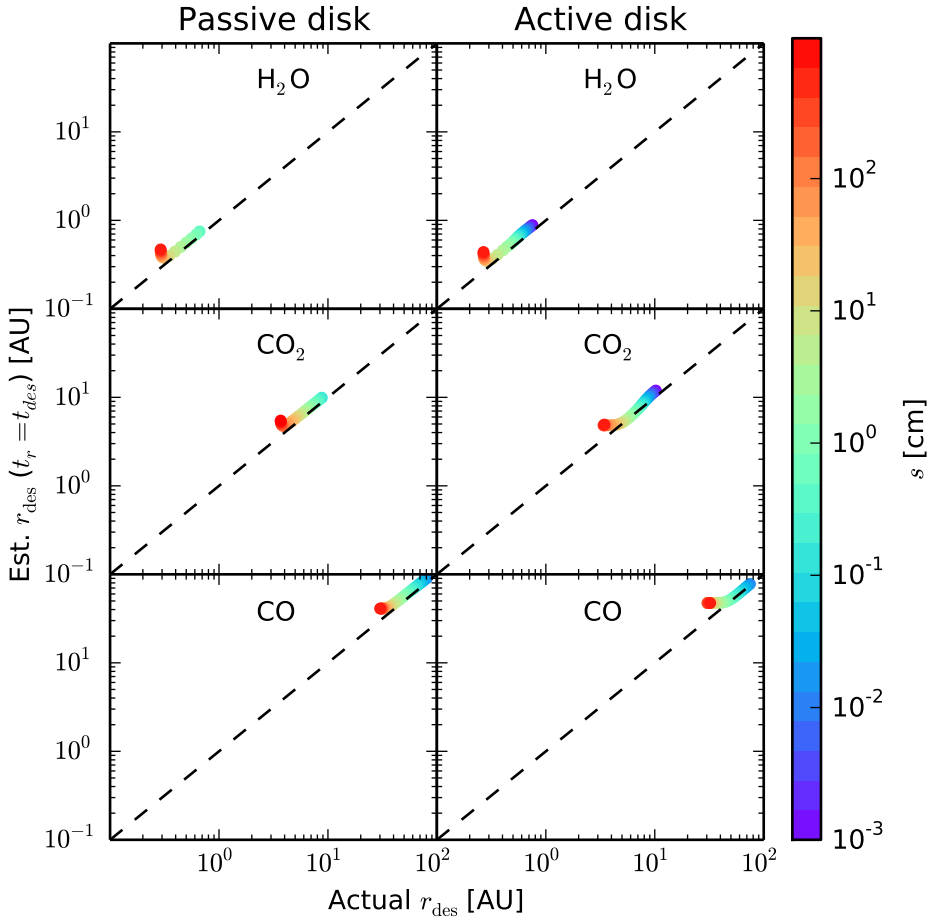

FIG. 3.— Desorption distance estimated from analytic calculations (see text) as a function of the desorption distance calculated numerically, for the range of particle sizes that desorb at a fixed distance regardless of their initial location (see Figure 2 and text). The estimate is performed for a passive disk (left panels) and an active disk (right panels). The particles are composed of H_2O (top panels), CO_2 (middle panels) and CO (bottom panels). The analytic approximation is in good agreement with the numerical result for most cases, with the exception of larger particles, $s \gtrsim 10$ cm (see text).

for a passive disk, an active disk with a passive temperature profile, and a steady-state active disk. The C/O ratio for a static disk is shown as a guideline. The plot is consistent with Figure 2. For the passive disk, only grains larger than ∼0.5 cm drift, desorb and thus move the snowline compared to the static disk. In contrast, even ∼micron-sized grains drift and desorb for the active disk, since they flow towards the host star together with the accreting gas. For the same particle size, the snowline locations are slightly closer to the central star in the active disk with a passive temperature profile, due to the fact that the accreting gas adds an additional component to the drift velocity of the solids (cf. Equation 12). The addition of accretional heating in the steady-state active disk moves the H_2O snowline outwards. This is due to the fact that accretional heating dominates in the inner disk, where high temperatures cause the grains to evaporate further away from the star. Once $r \gtrsim 1-2$ AU, stellar irradiation dominates the thermal evolution of the disk, and therefore the CO_2 and CO snowlines locations are the same as in the active disk with a passive temperature profile.

Perhaps the most interesting feature is the fact that the snowlines are pushed inwards as the grain size increases. While the plot only shows the snowlines and C/O ratio for particle sizes up to ∼7 m, we have found that almost kilometer-sized boulders are able to drift and desorb for both the passive and the active disk. Bodies larger than ∼7 m evaporate at the same location as the meter-sized planetesimals, though only the kilometer-sized boulders that are very close to the snownlines will contribute to determining the snowline location. Thus the innermost snowlines (depicted in red in Figure 5) set the limit on how close in the H_2O, CO_2 and CO snowlines can be pushed due to radial drift and gas accretion on to the host star. Realistic grain size distributions in disks are dominated by large grains (e.g., D'Alessio et al. 2001, Birnstiel et al. 2012). Therefore, the snowlines produced by the largest drifting solids in our model set the inner limit on the snowline locations and are insensitive to a particular grain size distribution.

For our choice of parameters, the snowline radii are:

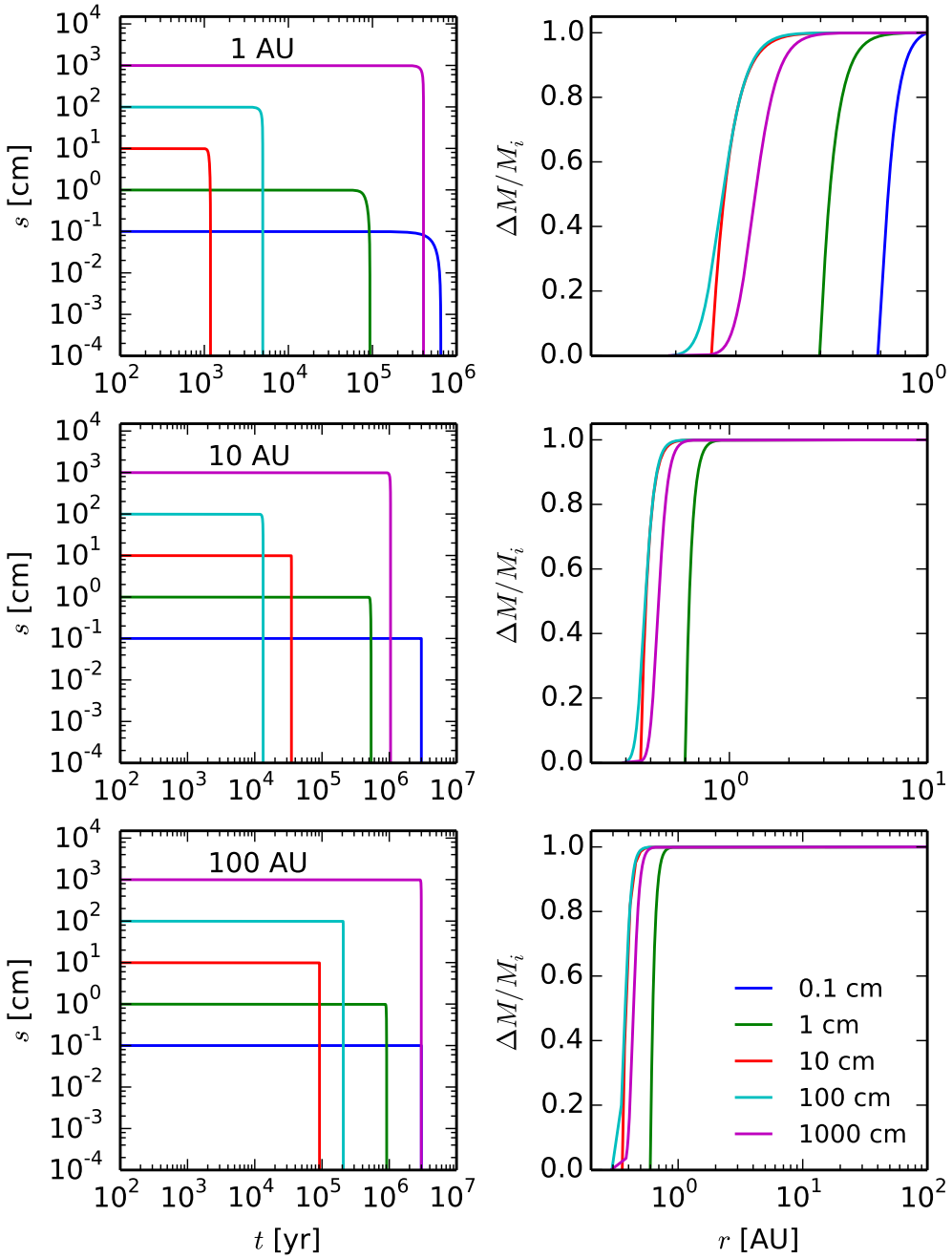

FIG. 4.— Left panels: size of desorbing H_2O particles as a function of time, for different initial particle sizes and for three initial locations in a passive disk: 1 AU (top left), 10 AU (middle left) and 100 AU (bottom left). Particles desorb almost instantaneously. Right panel: fractional mass of the desorbing particles as a function of the particle's location as it drifts, for different initial particle sizes, and at the same initial locations presented in the left panel. Particles lose most of their mass very close to the distance at which they fully desorb.

$r_{H_2O} \approx 0.3$ AU for the passive disk, $r_{H_2O} \approx 0.26$ AU for the active disk with a passive temperature profile and $r_{H_2O} \approx 0.63$ AU for the steady-state disk; $r_{CO_2} \approx 3.7$ AU for the passive disk, $r_{CO_2} \approx 3.4$ AU for both active disks; $r_{CO} \approx 30$ AU for the passive and both active disks. For comparison, $r_{H_2O} \approx 0.67$ AU, $r_{CO_2} \approx 8.6$ AU and

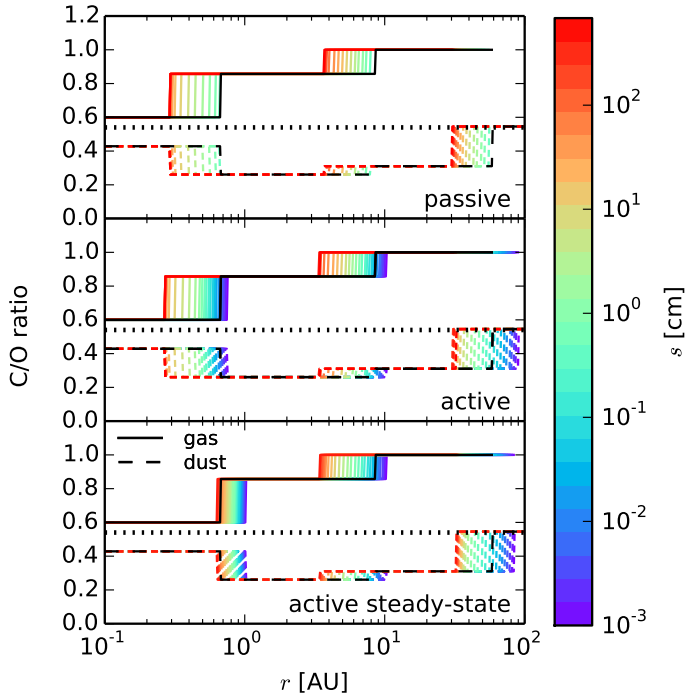

FIG. 5.— C/O ratio in gas (solid lines) and in dust (dashed lines) for a passive disk (top panel), an active disk with a passive temperature profile (middle panel) and a steady-state active disk (bottom panel), for the range of particle sizes that desorb at a fixed distance regardless of their initial location in the disk. The particle size increases from 0.001 cm to ∼700 cm as indicated by the color bar. The horizontal dotted line represents the stellar value of 0.54. The black lines represent the C/O ratio in gas (solid black line) and dust (dashed black line) for a static disk. The snowline location moves inward as the particle size increases.

$r_{CO} \approx 59$ AU for the static disk. Radial drift and gas accretion therefore push the snowline locations by up to ∼60 % for H_2O and CO_2, and by up to ∼50 % for CO.

5. DISCUSSION

5.1. *Generality of Results: Dependence on Disk Parameters*

In this section we investigate how variations in our fiducial parameters, such as the total disk mass or the time in the disk evolution at which we determine the snowline locations and the C/O ratio, affect our results. The disk lifetime $t_d = 3$ Myr is the most representative for our calculations, as this is the timeframe in which giant planets accrete their gaseous atmospheres (e.g., Pollack et al. 1996, Piso & Youdin 2014). However, protoplanetary cores start acquiring their envelope at earlier times, before the core is fully formed (e.g., Rafikov 2006). Recent models such as aerodynamic pebble accretion (Lambrechts & Johansen 2012) suggest rapid core growth on timescales of 10^5 years, which implies that the time when cores accrete their massive envelope may be at least an order of magnitude shorter than the disk lifetime. The composition of giant planet atmospheres, and specifically their C/O ratio, can thus depend on the abundance of H_2O, CO_2 and CO in gas and dust forms at earlier times than t_d in the disk evolution.

Figure 6 shows the desorption or final distance as a function of a particle's initial location in the disk, for grains of initial sizes of 10 cm and 1 m, composed of either H_2O, CO_2 or CO. These sizes are representative since radial drift timescales are shortest for particles within this size range (see Figure 1) — these are the particles whose drift and desorption evolution should be most strongly affected by variations in disk conditions. We stop the simulations after 10^4 yr, 10^5 yr, 1 Myr and $t_d = 3$ Myr, respectively, to see how the snowline locations evolve with time and affect the C/O ratio. Particles of a given size that start at large stellocentric distances do not desorb within the shorter timeframes, e.g. 10^4 or 10^5 years, but they do evaporate at a fixed radius if their initial location is closer to the host star. While the amount of material that moves through the disk changes with time, the radius at which particles desorb and thus the snowline locations are independent of the time elapsed. Therefore, our results are not only valid at t_d, but also throughout the earlier time evolution of the protoplanetary disk.

We choose as a fiducial model a total disk mass $M_d = 0.1 M_\odot$, but this number is not universally valid. From observations of the dust continuum, Andrews et al. (2013) find that a linear scaling $M_d \propto M_*$ is reasonable. Giant planets, however, have been detected around small stars (e.g., Montet et al. 2014), which can have masses as low as $M_* \sim 0.1 M_\odot$. We thus explore the effect of disk mass on the location of snowlines. Figure 7 shows the desorption or final distance as a function on the initial location of a H_2O particle with initial size of 1 m, for two total disk masses: $M_d = 0.1 M_\odot$, our fiducial model, and $M_d = 0.01 M_\odot$. The simulations are stopped after the same timeframes as those in Figure 6. The location of the H_2O snowline is the same for both disks (the same holds true for the CO_2 and CO snowlines). The C/O ratio is thus insensitive to the choice of M_d.

We also apply our active disk model to a transition disk, i.e. a protoplanetary disk with an inner cavity significantly depleted of gas. We choose a disk with an inner gap of radius $r_0 = 4$ AU, consistent with observations of TW Hya (Zhang et al. 2013), and with the gas surface density in the gap reduced by a factor of 1000. Figure 8 shows the desorption or final distance for a H_2O particle of initial size of 1 m, with the simulation stopped at the same timescales as in Figures 6 and 7. Particles that start at an initial distance interior to the gap drift towards the original snowline, while grains located exterior to the gap stop shortly after crossing the gap edge, due to the decrease in gas pressure inside the cavity, thus forming a snowline at ∼3.8 AU. This is consistent with the observations of Zhang et al. (2013), which show that the H_2O snowline is pushed outwards in a transition disk compared to a full disk.

5.2. *Model Extensions*

Our goals in this paper were (1) to gain a detailed qualitative and quantitative understanding of the effect of radial drift and gas accretion onto the central star on snowline locations and the C/O ratio in disks, and (2) to obtain a limit on how close in the snowlines can be pushed due to drift and gas accretion. We have thus used a simplified model and out of necessity neglected potentially significant dynamical and chemical processes. In what follows, we discuss these limitations and their

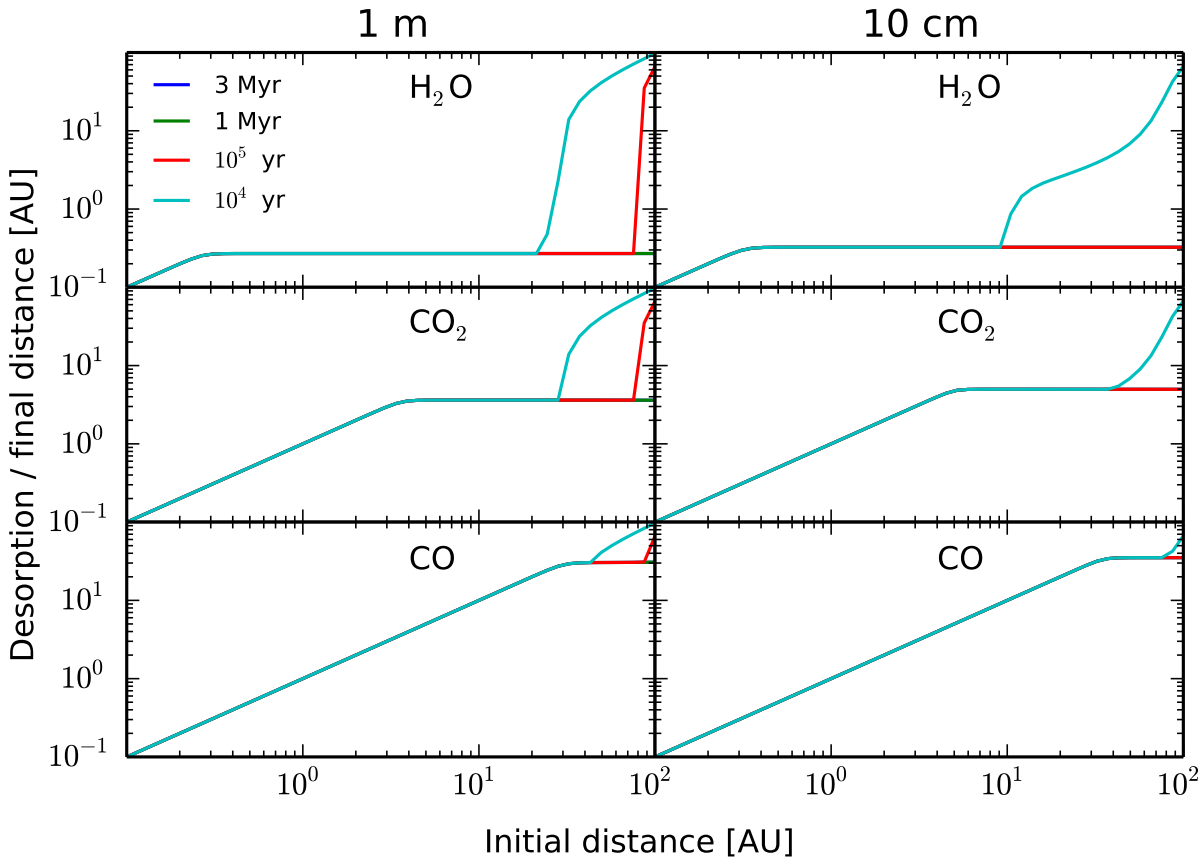

FIG. 6.— Desorption / final distance as a function of initial position in the disk for particles of initial size $s_0 = 1$ m (left panels) and $s_0 = 10$ cm (right panels), for grains composed of H_2O (top panels), CO_2 (middle panels) and CO (bottom panels). The evolution is shown at four representative timescales: 10^4 yr (cyan curve), 10^5 yr (red curve), 1 Myr (green curve), and 3 Myr, the disk lifetime (blue curve). For a given particle size, the desorption distance, and hence the H_2O, CO_2 and CO snowlines, have the same location regardless of the time at which the simulation is stopped.

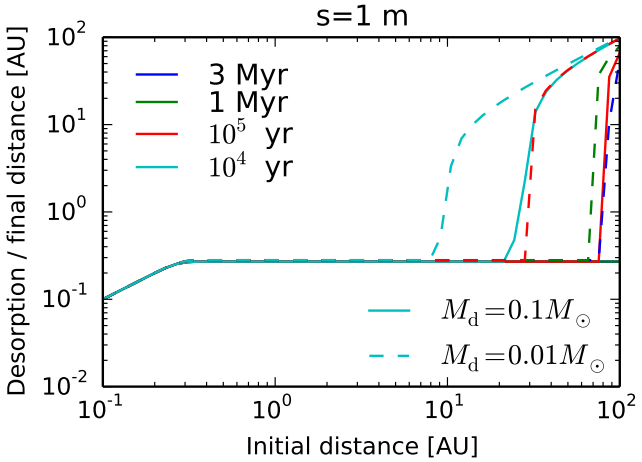

FIG. 7.— Desorption / final distance as a function of initial position in the disk for H_2O particles of initial size of 1 m, for total disk masses $M_d = 0.1M_\odot$ (solid lines) and $M_d = 0.01M_\odot$ (dashed lines). The timescales of the simulations and their color code are the same as in Figure 6. A lower disk mass does not change the snowline location.

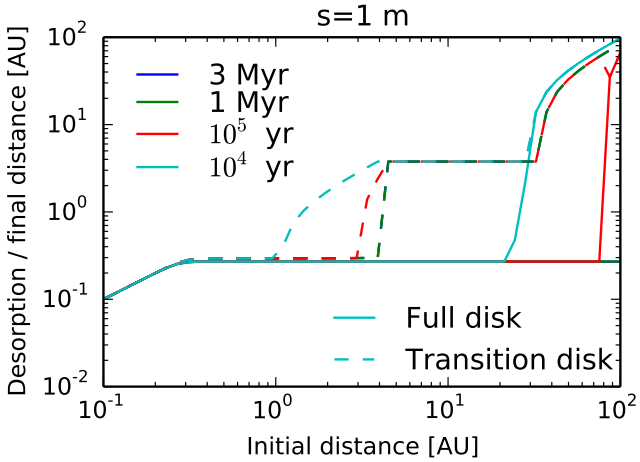

FIG. 8.— Desorption / final distance as a function of initial position in the disk for H_2O particles of initial size of 1 m, for our fiducial disk (solid lines) and for a transition disk with an inner cavity at $r_0 = 4$ AU (dashed lines). The timescales of the simulations and their color code are the same as in Figure 6. Particles that start inside the cavity drift towards the original snowline, while particles that start outside the gap stop shortly after crossing the gap edge.

effects. We note that our future work will address some

TABLE 1
The effects of dynamical and chemical processes on snowline shapes and locations

Process	Effect
Radial drift	← [a]
Gas accretion	←
Particle growth	→
Turbulent diffusion	→ ←
Particle fragmentation	→ ←
Grain morphology	→
Particle composition	→ ←
Disk gaps and holes	→
Non-static chemistry	→ ←

[a]The arrows signify how a process affects the snowline: ← means that the snowline is pushed closer to the host star, → means that the snowline is pushed further from the host star. The presence of both arrows means that the process may have both effects on the snowline location.

of these issues.

We summarize in Table 1 the potential physical and chemical processes occurring in disks and their effect on snowline locations. For the sake of completion, Table 1 also includes the processes addressed in this paper, i.e. radial drift and gas accretion. The neglected effects are discussed in more detail below.

1. **Particle growth.** While our model assumes a range of particle sizes, each size is considered fixed for a given grain throughout its drift and evolution. However, grain growth has been observed in protoplanetary disks (e.g., Ricci et al. 2010, Pérez et al. 2012), as well as theoretically constrained (e.g., Birnstiel et al. 2010, Birnstiel et al. 2012). In Section 4 we have shown that larger grains move the snowline locations closer in, but those locations remain fixed above a certain particle size. Particle growth will thus initially push the snowlines inwards. However, once the solids grow larger than km-sized, they are no longer affected by drift or desorption, and the snowline reduces to that of a static disk. It follows that grain growth will eventually push the snowline location outwards.

2. **Turbulent diffusion.** The radial drift model presented in Section 2.2 only considers a laminar flow and thus ignores turbulence. However, the disk gas also experiences turbulent diffusion (e.g., Birnstiel et al. 2012, Ali-Dib et al. 2014). Turbulence causes eddies and vertical mixing, which are likely to reduce the radial gas accretion velocity. Additionally, the flow of H_2O, CO_2 and CO vapor will diffuse radially. Back-diffusion across the snowline will change the shape of the snowline, as well as the C/O ratio in gas and dust both inside and outside of the snowline, due to the reduction of gas-phase volatile abundance interior to the snowline.

3. **Particle fragmentation.** Frequent particle collisions in disks cause them to fragment (e.g., Birnstiel et al. 2012). The fragmentation of meter- to km-sized particles will move the snowlines outwards, as smaller particles desorb faster and further out from the host star (cf. Figures 2 and 5). Large boulders, which neither drift nor desorb, may become e.g. meter-sized due to collisions and subsequent fragmentation, which will cause them to drift significantly before desorbing, pushing the snowlines inwards. Thus fragmentation can move the snowline locations in either radial direction.

4. **Grain morphology.** Our model assumes that the ice particles are perfect, homogeneous spheres. However, this is not a very good approximation, since grain growth can be fractal rather than compact (Zsom et al. 2010, Okuzumi et al. 2012). The inhomogeneity due to cracks in the grain structure will cause the particles to desorb faster. They will therefore drift less before evaporating and will move the snowlines outwards.

5. **Particle composition.** The ice particles in our model are assumed to be fully formed of either H_2O, CO_2 or CO. In reality, the grains have a layered structure, such as an interior composed of non-volatile materials (e.g., sillicates) covered by an icy layer. The ice thus only constitutes a fraction of the total particle mass, which accelerates its desorption and pushes the snowlines outwards. The grains may also be composed of a mixture of H_2O, CO_2 and CO ices. In this case, the desorption energies are largest for the most volatile species, which will move the snowlines inwards.

6. **Disk gaps and holes.** The snowline locations will be different for transition disks, which have inner cavities significantly depleted of gas (e.g., Espaillat et al. 2012), or pre-transitional disks, which have a gap between an inner and outer full disk (e.g., Kraus et al. 2011). The decrease in gas pressure in these gaps or holes will reduce the particles' drift velocity close to the gap edge, thus slowing them down and pushing the snowline outwards.

7. **Non-static chemistry.** As the goal of this paper was to explore only the dynamical effects on snowline locations and the C/O ratio in disks, we have assumed a simple, static chemical model. However, gas-grain chemistry is very complex and time-dependent. In the inner disk, chemistry approaches equilibrium due to intense sources of ionizing radiation (e.g., Ilgner et al. 2004), while in the outer disk high energy radiation and cosmic rays are the key drivers of chemistry, which is no longer in equilibrium (e.g., van Dishoeck 2006). A multitude of chemical evolution models have been developed (see references in Henning & Semenov 2013), many of which contain tens or hundreds of chemical reactions. Due to the complexity of these chemical models, most of them are decoupled from disk dynamics. The effect of disk chemistry on snowline locations, shape, time evolution, or the C/O ratio is therefore difficult to estimate. In a future paper, we plan to use a parametrized chemical model and incorporate it in our radial drift calculation.

6. SUMMARY

We study the effect of radial drift of solids and viscous gas accretion onto the central star on the H_2O,

CO_2 and CO snowline locations and the C/O ratio in a protoplanetary disk, assuming static chemistry. We develop a simplified model to describe the coupled drift-desorption process and determine the time evolution of particles of different sizes throughout the disk. We assume that the solid particles are perfect, homogeneous spheres, fully composed of either H_2O, CO_2 or CO. We apply our model to a passive disk, an active disk with a passive temperature profile, and a steady-state active disk that also takes into account stellar irradiation. We determine the desorption or final location of drifting particles after a time equal to the disk lifetime, and use this result to set an inner limit for the location of the H_2O, CO_2 and CO snowlines. Our results can be summarized as follows:

1. Radial drift and gas accretion affect desorption and move the snowline locations compared to a static disk for particles with sizes $\sim$0.5 cm $\lesssim s \lesssim$ 7 m for a passive disk and $\sim$0.001 cm $\lesssim s \lesssim$ 7 m for an active disk. Moreover, boulders up to almost kilometer-size contribute to setting the snowline locations if they are very close to the snowlines.

2. Particles with sizes in the above range desorb instantaneously, and at a fixed location in the disk that only depends on the particle size. Thus for each particle size there is a fixed and uniquely determined H_2O, CO_2 or CO snowline.

3. The results of the numerical simulation are in agreement with the analytic solution of the drift-desorption system of differential equations if the stopping time $\tau_s \ll 1$. We present an explicit analytic solution for the desorption distance in this regime.

4. The snowline locations move inwards as the particle size increases; the innermost snowline is set by particles with initial size $s \sim 7$ m. Gas accretion causes even micron-sized particles to drift, desorb and move the snowline location compared to a static disk. A steady-state disk that includes accretion heating moves the H_2O snowline outwards compared to an active disk with a passive temperature profile, but has no effect on the CO_2 and CO snowline locations.

5. Since realistic grain size distributions are dominated by the largest particles, the H_2O, CO_2 and CO snowlines are those created by the largest drifting particles in our model. This corresponds to the innermost snowlines that we determine. Our model thus sets a limit on how close to the central star the snowlines can be pushed by radial drift and gas accretion.

6. For our fiducial model, the innermost H_2O, CO_2 and CO snowlines are located at 0.3 AU, 3.7 AU and 30 AU for a passive disk, 0.26 AU, 3.4 AU and 30 AU for an active disk with a passive temperature profile, and 0.63 AU, 3.4 AU and 30 AU for a steady-state active disk. Compared to a static disk, radial drift and gas accretion move the snowlines by up to 60 % for H_2O and CO_2, and by up to 50 % for CO.

7. Our model finds that the C/O ratio is enhanced compared to the stellar value throughout most of the disk, with the C/O ratio reaching unity between the CO_2 and CO snowlines. This is consistent with observations of C/O ratios in some exoplanet atmospheres.

8. The snowline locations are independent of the time at which we stop our simulation and of the total disk mass. Our results are thus valid throughout the evolution of the gas disk, not only after the disk has dissipated, which has implications on the composition of nascent giant planets.

Our model does not address additional effects, such as gas diffusion, grain composition and morphology, or complex time-dependent chemical processes. Future work will address some of these dynamical and chemical processes, with the goal of obtaining more realistic results for the snowline locations, shapes and time evolution, and the resulting effect on the C/O ratio.

APPENDIX

STEADY-STATE ACTIVE DISK SOLUTION

Following Shakura & Sunyaev (1973) and Armitage (2010), the steady-state solution for a thin actively accreting disk with an α-prescription for viscosity is governed by the following set of equations:

$$\nu = \alpha c_\mathrm{d} H_\mathrm{d} \tag{A1a}$$

$$c_\mathrm{d}^2 = \frac{k_\mathrm{B} T_\mathrm{d,act}}{\mu m_\mathrm{p}} \tag{A1b}$$

$$\rho_\mathrm{d} = \frac{1}{\sqrt{2\pi}} \frac{\Sigma_\mathrm{d}}{H_\mathrm{d}} \tag{A1c}$$

$$H_\mathrm{d} = \frac{c_\mathrm{d}}{\Omega_k} \tag{A1d}$$

$$T_\mathrm{d,act}^4 = \frac{3}{4} \tau T_\mathrm{d,surf}^4 \tag{A1e}$$

$$\tau = \frac{1}{2} \Sigma_\mathrm{d} \kappa \tag{A1f}$$

$$\nu\Sigma_{\rm d} = \frac{\dot{M}}{3\pi} \tag{A1g}$$

$$\sigma T_{\rm d,surf}^4 = \frac{9}{8}\nu\Sigma_{\rm d}\Omega_{\rm k}^2 \tag{A1h}$$

$$\kappa = \kappa_0 T_{\rm d,act}^2, \tag{A1i}$$

where $T_{\rm d,surf}$ is the surface temperature of the disk and the other quantities are defined in the main text. This is a system of nine equations with nine unknowns (ν, $c_{\rm d}$, $H_{\rm d}$, $T_{\rm d,act}$, $\rho_{\rm d}$, $\Sigma_{\rm d}$, τ, $T_{\rm d,surf}$, κ) that can be solved numerically once α and κ_0 are specified.

DESORPTION DISTANCE ANALYTIC SOLUTION

For a particle of size s that desorbs and satisfies $\tau_{\rm s} \ll 1$ ($\tau_{\rm s}$ is the dimensionless stopping time, defined in Section 2.2), we can derive an explicit analytic solution for the particle's desorption distance in a passive disk. For $\tau_{\rm s} \ll 1$, a particle is in the Epstein drag regime (see Equation 9) and its drift velocity $\dot{r}$ (Equation 10) can be approximated as

$$\dot{r} \approx -2\eta\Omega_{\rm k} r \tau_{\rm s}. \tag{B1}$$

By using Equations (15) and (16) and setting $t_{\rm r,drift} = t_{\rm des}$, we can express a particle's desorption distance as

$$r_{\rm des} = \left(\frac{d\, \mathcal{W}\left[\frac{(B/A)^{-q/d} q\, C}{d} q C \right]}{q\, C} \right)^{\frac{1}{q}}, \tag{B2}$$

where $\mathcal{W}$ is the Lambert-W function, $q = 3/7$ is the power-law coefficient in Equation (1b), $d = -\frac{1}{2} + p - q$ with $p = 1$ the power-law coefficient in Equation (1a), and

$$A = \frac{\rho_0}{\rho_{\rm s}} \frac{r_0^2}{s c_0} r_0^d \tag{B3a}$$

$$B = \frac{\rho_{\rm s} s}{3\mu_{\rm x} N_{\rm x} \nu_{\rm x}} \tag{B3b}$$

$$C = \frac{E_{\rm x}}{T_0} r_0^{-q}, \tag{B3c}$$

(B3d)

where $r_0 = 1$ AU, $\rho_0 = \rho_{\rm d}(r_0)$ and $c_0 = c_{\rm d}(r_0)$.

REFERENCES

Ali-Dib, M., Mousis, O., Petit, J.-M., & Lunine, J. I. 2014, ApJ, 785, 125

Andrews, S. M., Rosenfeld, K. A., Kraus, A. L., & Wilner, D. J. 2013, ApJ, 771, 129

Andrews, S. M., Wilner, D. J., Hughes, A. M., Qi, C., & Dullemond, C. P. 2010, ApJ, 723, 1241

Armitage, P. J. 2010, Astrophysics of Planet Formation

Bell, K. R. & Lin, D. N. C. 1994, ApJ, 427, 987

Birnstiel, T., Dullemond, C. P., & Brauer, F. 2010, A&A, 513, A79

Birnstiel, T., Klahr, H., & Ercolano, B. 2012, A&A, 539, A148

Chiang, E. & Youdin, A. N. 2010, Annual Review of Earth and Planetary Sciences, 38, 493

D'Alessio, P., Calvet, N., & Hartmann, L. 2001, ApJ, 553, 321

Du, F., Bergin, E. A., & Hogerheijde, M. R. 2015, ArXiv e-prints

Espaillat, C., Ingleby, L., Hernández, J., Furlan, E., D'Alessio, P., Calvet, N., Andrews, S., Muzerolle, J., Qi, C., & Wilner, D. 2012, ApJ, 747, 103

Frank, J., King, A., & Raine, D. J. 2002, Accretion Power in Astrophysics: Third Edition

Hartmann, L., Calvet, N., Gullbring, E., & D'Alessio, P. 1998, ApJ, 495, 385

Henning, T. & Semenov, D. 2013, Chemical Reviews, 113, 9016

Hollenbach, D., Kaufman, M. J., Bergin, E. A., & Melnick, G. J. 2009, ApJ, 690, 1497

Ilgner, M., Henning, T., Markwick, A. J., & Millar, T. J. 2004, A&A, 415, 643

Kraus, A. L., Ireland, M. J., Martinache, F., & Hillenbrand, L. A. 2011, ApJ, 731, 8

Lambrechts, M. & Johansen, A. 2012, A&A, 544, A32

Madhusudhan, N., Amin, M. A., & Kennedy, G. M. 2014, ApJ, 794, L12

Madhusudhan, N., Harrington, J., Stevenson, K. B., Nymeyer, S., Campo, C. J., Wheatley, P. J., Deming, D., Blecic, J., Hardy, R. A., Lust, N. B., Anderson, D. R., Collier-Cameron, A., Britt, C. B. T., Bowman, W. C., Hebb, L., Hellier, C., Maxted, P. F. L., Pollacco, D., & West, R. G. 2011, Nature, 469, 64

Montet, B. T., Crepp, J. R., Johnson, J. A., Howard, A. W., & Marcy, G. W. 2014, ApJ, 781, 28

Mordasini, C., Klahr, H., Alibert, Y., Miller, N., & Henning, T. 2014, A&A, 566, A141

Öberg, K. I., Murray-Clay, R., & Bergin, E. A. 2011a, ApJ, 743, L16

Öberg, K. I., Qi, C., Fogel, J. K. J., Bergin, E. A., Andrews, S. M., Espaillat, C., van Kempen, T. A., Wilner, D. J., & Pascucci, I. 2010, ApJ, 720, 480

Öberg, K. I., Qi, C., Fogel, J. K. J., Bergin, E. A., Andrews, S. M., Espaillat, C., Wilner, D. J., Pascucci, I., & Kastner, J. H. 2011b, ApJ, 734, 98

Öberg, K. I., Qi, C., Wilner, D. J., & Andrews, S. M. 2011c, ApJ, 743, 152

Okuzumi, S., Tanaka, H., Kobayashi, H., & Wada, K. 2012, ApJ, 752, 106

Pérez, L. M., Carpenter, J. M., Chandler, C. J., Isella, A., Andrews, S. M., Ricci, L., Calvet, N., Corder, S. A., Deller, A. T., Dullemond, C. P., Greaves, J. S., Harris, R. J., Henning, T., Kwon, W., Lazio, J., Linz, H., Mundy, L. G., Sargent, A. I., Storm, S., Testi, L., & Wilner, D. J. 2012, ApJ, 760, L17

Piso, A.-M. A. & Youdin, A. N. 2014, ApJ, 786, 21

Pollack, J. B., Hubickyj, O., Bodenheimer, P., Lissauer, J. J., Podolak, M., & Greenzweig, Y. 1996, Icarus, 124, 62

Qi, C., D'Alessio, P., Öberg, K. I., Wilner, D. J., Hughes, A. M., Andrews, S. M., & Ayala, S. 2011, ApJ, 740, 84

Rafikov, R. R. 2006, ApJ, 648, 666

Ricci, L., Testi, L., Natta, A., & Brooks, K. J. 2010, A&A, 521, A66

Shakura, N. I. & Sunyaev, R. A. 1973, A&A, 24, 337
Thiabaud, A., Marboeuf, U., Alibert, Y., Leya, I., & Mezger, K. 2015, A&A, 574, A138
van Dishoeck, E. F. 2006, Proceedings of the National Academy of Science, 103, 12249
Weidenschilling, S. J. 1977, MNRAS, 180, 57
Zhang, K., Pontoppidan, K. M., Salyk, C., & Blake, G. A. 2013, ApJ, 766, 82
Zsom, A., Ormel, C. W., Güttler, C., Blum, J., & Dullemond, C. P. 2010, A&A, 513, A57